RSC Advances

PAPER

View Article Online
View Journal | View Issue

Cite this: *RSC Adv.*, 2025, **15**, 49739

β-caryolane derivatives as novel anti-colorectal cancer agents: synthesis and *in vitro* biological evaluation

Xingjun Xu, †[ab] Zhiwei Wang, †[ab] Anjie Huang,[b] Zhongjing Qiao,[b] Yonglin Ge,[b] Hui Wen,[b] Junxiang Cheng,[b] Yaopeng Zhao*[ab] and Xinmiao Liang *[ab]

β-Caryolane derivatives possess a unique skeletal structure and a wide range of practical applications. Recent studies suggest that certain β-caryolane derivatives may exhibit enhanced anti-colorectal cancer activity compared to their natural parent compounds, β-caryolanol and β-caryophyllene (β-CP). However, the structural diversity of known β-caryolane derivatives remains limited, likely due to challenges in their synthesis. In this study, we systematically investigated, for the first time, the reactivity of three nucleophiles (sulfonamides, amides, and azide) with β-CP under acid catalysis. The corresponding β-caryolane-type products were successfully obtained in a single step. The azide-addition product further underwent click reactions with various alkynes to yield triazole derivatives. Compared to β-CP or β-caryolanol, most amino-substituted β-caryolane derivatives demonstrated significantly improved anti-proliferative activity against several colorectal cancer cell lines, especially HT-29 cells. Among them, compound **NC-19** showed the most potent antiproliferative effect against HT-29 cells with an IC_{50} of 2.496 ± 0.255 μM. Preliminary pharmacological mechanism studies indicated that **NC-19** induces apoptosis, arrests the cell cycle at the G0/G1 phase, significantly increases intracellular ROS levels and suppresses cell migration in HT-29 cells. These results expanded the chemical diversity of bioactive β-caryolane derivatives and offered new options for the development of anti-colorectal cancer agents.

Received 26th September 2025
Accepted 1st December 2025

DOI: 10.1039/d5ra07312j

rsc.li/rsc-advances

1 Introduction

Colorectal cancer (CRC) is one of the most common malignant tumors worldwide, typically arising from the abnormal proliferation and malignant transformation of cells in the colon lining.[1,2] Due to its high incidence and mortality rates, CRC imposes a heavy burden on both healthcare systems and affected patients.[3] Although the availability of conventional treatment methods including surgery, radiotherapy, chemotherapy and targeted therapies, the unsatisfactory therapeutic effects and high costs continue to present major challenges in CRC management. The incidence of CRC is expected to rise in the coming years, according to the World Health Organization, which makes the development of more targeted and effective treatments an urgent priority.[1,4,5]

Medicinal plants and their active compounds have long been recognized as important sources for drug research and development due to their diverse molecular skeletons and broad spectrum of biological activities, particularly in the field of anticancer therapeutics.[6–8] β-Caryophyllene (β-CP) is a bicyclic sesquiterpene widely distributed in the essential oils of various plants such as basil, cinnamon, black pepper and rosemary,[9] and is usually used as food additives and flavoring agents.[10] It was reported that β-CP and its natural analogues (mainly caryophyllene oxide, β-CPO) are able to induce apoptosis of various human cancer cells and prevent their proliferation and metastasis through multiple pathways.[11–13] Especially for CRC, β-CP can selectively exert antiproliferative activity by disrupting mitochondrial membrane potential, inhibiting angiogenesis, and blocking the action of mono-ADP-ribosyltransferase 1 (ART1).[14,15] Furthermore, β-CP can enhance chemosensitization to paclitaxel by promoting drug accumulation in cancer cells.[16–18]

Due to its highly strained cyclobutyl ring, along with one cyclic double bond at the C4-site and one exocyclic double bond at the C8-site of cyclononyl moiety, β-CP is frequently employed as a synthetic substrate for the preparation of various functional molecules and polymer materials.[19] The most common reaction involving β-CP is acid-catalyzed nucleophilic addition followed

[a]*State Key Lab of Phytochemistry and Natural Medicines, Dalian Institute of Chemical Physics, CAS, Dalian 116023, China. E-mail: liangxm@dicp.ac.cn; ypzhao@dicp.ac.cn; Fax: +86-411-84379539; Tel: +86-411-84379519*

[b]*Jiangxi Provincial Key Laboratory for Pharmacodynamic Material Basis of Traditional Chinese Medicine, Ganjiang Chinese Medicine Innovation Center, Nanchang, 330000, China*

† Xingjun Xu and Zhiwei Wang were contributed equally to this work.

by *trans*-annular rearrangement (Fig. 1A). Since both double bonds can participate in *trans*-annular rearrangement reactions and these transformations proceed readily, the resulting products often consist of complex mixtures of polycyclic products. Among these, tricyclic sesquiterpenoid β-caryolane-type compounds, such as β-caryolanol and its derivatives, are common products and are typically used as fragrance ingredient.[20–22] In addition, β-caryolanol has been reported to exhibit antiasthmatic, antitussive, expectorant and anticancer effects.[23,24] Recently, we found that β-caryolane derivatives containing amino substituents demonstrate more potent antiproliferative activity against various cancer cells lines compared to β-CP and β-caryolanol. Pharmacological studies indicate that these derivatives significantly inhibit the growth of CRC cells and tumors, exhibiting *in vitro* and *in vivo* efficacy comparable to 5-FU. The underlying mechanism may involve G0/G1 cell cycle arrest, enhanced ROS accumulation leading to DNA damage, apoptosis, autophagy, NF-κB pathway activation and PI3K/Akt/mTOR pathway suppression. These findings position β-caryolane amino derivatives as a promising novel class of compounds with confirmed anti-CRC activity.[24]

β-caryolane derivatives can be prepared directly from β-CP. However, perhaps due to synthetic challenges, the structural diversity of reported β-caryolane derivatives remains limited (Fig. 1B). In the presence of H_2O, alcohol, phenol, acetic anhydride or acetic acid, the acid-catalyzed reactions of β-CP yield β-caryolanol, β-caryolanyl acetate or β-caryolanyl ether derivatives (**1**).[25–28] When clays or zeolites are used catalysts, phenol reacts with β-CP to give β-caryolanyl benzene (**2**) *via* Friedel–Crafts alkylation.[29] The Ritter reaction of β-CP with acetonitrile produces β-caryolanyl acetamide (**3**),[30] and the hydroamination with 2,2,2-trifluoroethyl sulfamate produces β-caryolanyl sulfonamide (**4**).[31] Although these reactions proceed in one step, they are often accompanied by the formation of multiple by-products, resulting in low yields for most target products.

Given the promising anti-CRC activity of β-caryolane derivatives reported in the literature, we sought to further expand their structural diversity and provide novel compounds for anticancer studies. In this work, we developed three new one-step methods for synthesizing β-caryolane derivatives. The obtained derivatives were evaluated for their antiproliferative activity against several CRC cell lines, including HT-29, HCT-116, and HCT-15. The representative compound was selected to study its preliminary pharmacological properties.

2 Results and discussion

2.1 Chemistry

As the main product of the acid-catalyzed rearrangement reaction of β-CP, the formation mechanism of β-caryolane derivatives is illustrated in Fig. 1A. At room temperature, β-CP exists as a mixture of four conformers separated by a low barrier of inversion, βα (75%), ββ (21%), αα (3%) and αβ (<1%).[25,29] Among four conformers, the ββ is most susceptible to protonation at the endocyclic double bond under acid catalysis, thereby generating a tertiary carbocation. Steric hindrance around the carbocation prevents direct attack by external nucleophiles, instead driving a transannular reaction with the spatially adjacent exocyclic double bond to form a bridgehead carbocation. The reduced steric congestion at the bridgehead center allows nucleophiles to engage in highly selective attack, leading to the formation of β-caryolane derivatives.[25,32] This high stereoselectivity originates from the preorganized geometric

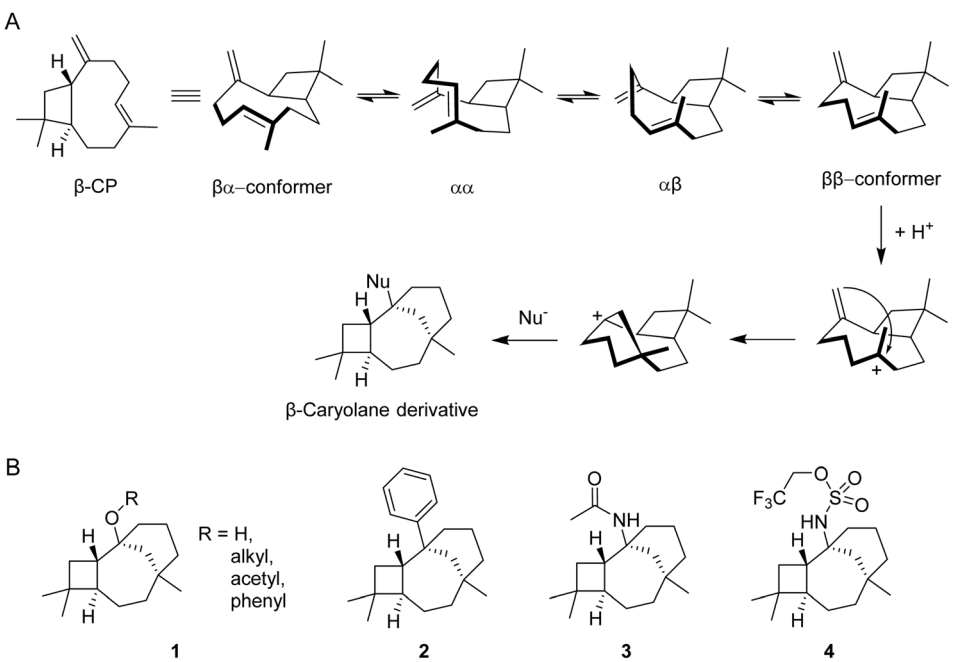

Fig. 1 (A) Acid-catalyzed reaction mechanism for the conversion of β-CP to β-caryolane derivatives. (B) The structures of reported β-caryolane derivatives directly prepared from β-CP.

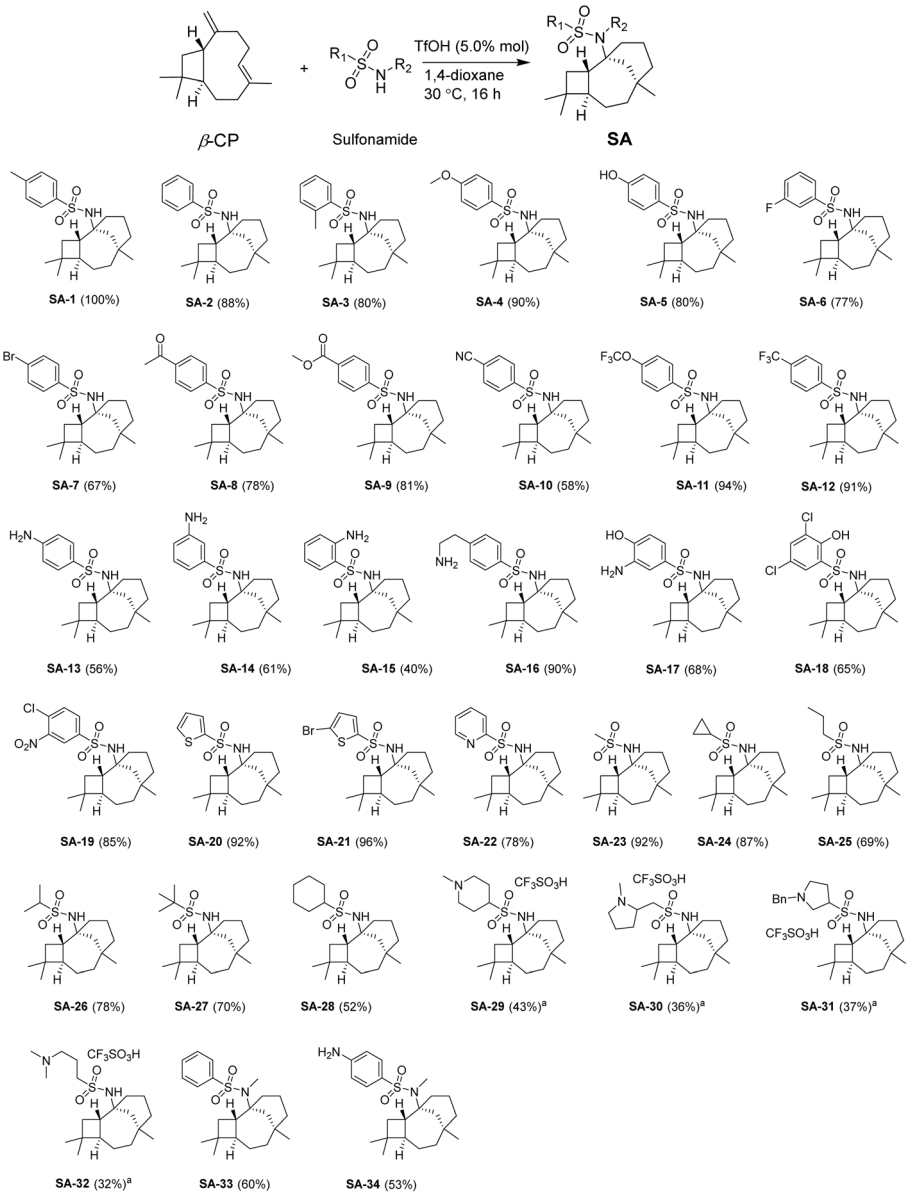

Scheme 1 Substrate scope for the synthesis of N-β-caryolanyl-sulfonamide derivatives **SA**. Reactions were performed at 30 °C for 16 h under air atmosphere using β-CP (0.2 mmol), sulfonamide (0.1 mmol), and 1,4-dioxane (2 mL), with TfOH (5.0% mol) as catalyst.

conformation of the substrate during the critical transannular step. Common nitrogen-based nucleophiles in acidic media include sulfonamides, amides, azides, and related compounds. Given the critical role of nitrogen atoms in drug molecules, we are particularly interested in exploring the feasibility of employing such nucleophiles to facilitate the conversion of β-CP into nitrogen-containing β-caryolane derivatives.

Initially, *p*-toluenesulfonamide ($TsNH_2$) was chosen as nucleophilic substrate to react with β-CP, using trifluoromethanesulfonic acid (TfOH) as the acid catalyst. As expected, the reaction produced a tricyclic sesquiterpenoid compound **SA-1** with a N-β-caryolanyl-*p*-toluenesulfonamide structural moiety. The structure of **SA-1** was confirmed by HRMS and NMR spectra. Furthermore, X-ray crystallography unambiguously established the absolute configuration of **SA-1** (CCDC 1942093); the detailed crystallographic data are presented in Table S1. Among the catalysts screened, TfOH gave the best yield (74%, based on $TsNH_2$), outperforming TsOH, TFA, H_2SO_4, $AlCl_3$, and BF_3 Et_2O. Increasing β-CP from 2.0 to 5.0 equiv. relative to $TsNH_2$ boosted the yield from 74% to 100%, but also resulted in more side reactions, evident from the complete consumption of the excess β-CP. The optimal temperature was 30 °C; lower (20 °C) or higher (80 °C) temperatures reduced or did not improve the yield. Based on a comprehensive evaluation of the parameters in Table S2 to balance reaction yield and material efficiency, the optimized conditions were determined to be a 2 : 1 ratio of β-CP to $TsNH_2$ in 1,4-dioxane at 30 °C for 16 hours, which were subsequently employed for further research.

Employing the optimized reaction conditions, we explored the substrate scope of sulfonamides. As shown in Scheme 1,

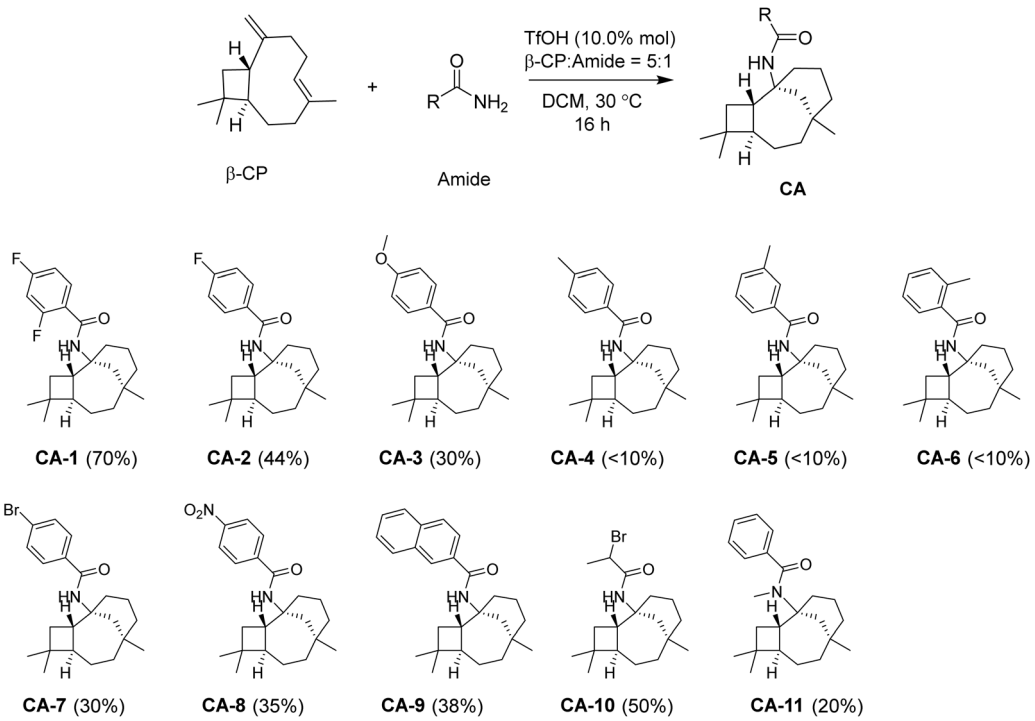

Scheme 2 Substrate scope for the synthesis of N-β-caryolanyl-amides derivatives **CA**. Reactions were performed at 30 °C for 16 h under air atmosphere using β-CP (5.0 equiv.), amide (0.1 mmol, 1.0 equiv.), and DCM (2 mL), with TfOH (10.0% equiv.) as catalyst.

a wide range of functional groups and substituents were tolerated for this reaction. The benzene sulfonamides substituted by electron-withdrawing or electron-donating groups reacted well with β-CP and gave good to excellent yields (**SA-1**-**SA-19**). Heterocyclic arylsulfonamides or alkyl sulfonamides also underwent the transformation successfully, yielding the corresponding products with high yields (**SA-20**-**SA-32**). It was worth noting that for an alkaline amino substrate, an excess of TfOH catalyst was necessary (1.05 equiv. of TfOH was used here), leading to the formation of the corresponding salt products in moderate yields, such as **SA-29**-**SA-32**. When *N*-methylsulfonamide was used as substrates, the reaction also proceeded smoothly in moderate yields (**SA-33** and **SA-34**).

The amide bond is a common structural motif in the design and synthesis of pharmaceutical compounds. Although a recent literature reports that acetonitrile and β-CP can react directly to form β-caryolanyl acetamide, the structural diversity of products from this reaction remains limited.[22,29] We therefore tried to extend the acid-catalyzed reaction of β-CP to the synthesis of β-caryolanyl amides. However, under the optimized reaction conditions established in Scheme 1, the reaction between 2,4-difluorobenzamides and β-CP failed to produce the desired β-caryolanyl amides. The desired product **CA-1** was obtained in 70% yield only when DCM was employed as solvent, and the loadings of both the TfOH catalyst and β-CP were increased to 0.1 and 5.0 equivalents, respectively (Scheme 2). Under these conditions, various other benzamides and alkylamides also successfully underwent acid-catalyzed reactions with β-CP, producing the corresponding N-β-caryolanyl-amide products (**CA-2** to **CA-10**) in low to moderate yields. Additionally, *N*-methylbenzamide reacted with β-CP to give **CA-11** in 20% yield. The relatively low yields compared to those obtained with sulfonamides may be attributed to the weaker nucleophilicity of amides.

In pharmaceutical synthesis, azide compounds are widely employed as versatile building blocks due to their exceptional reactivity and selectivity.[33] To facilitate the integration of β-caryolane scaffolds into diverse bioactive structures, we explored the use of azido groups as nucleophiles for β-CP functionalization. Based on the optimized reaction conditions from Scheme 1, we firstly used trimethylsilyl azide ($TMSN_3$) as azidation reagent to run the hydroazidation of β-CP. The desired β-caryolane-azide product **NC** was obtained in 92% yield (Table S3). In contrast, alternative azide sources such as sodium azide (NaN_3) and diphenylphosphoryl azide (DPPA) proved less effective, each yielding the product in only approximately 40%. Subsequent reaction optimization revealed that DCM is a more effective solvent than 1,4-dioxane, affording a superior yield (96% *vs.* 91%). Furthermore, the reaction reached completion within 8 hours.

Employing compound **NC** as a versatile building block, we successfully synthesized a series of triazole derivatives *via* reactions with alkynes. The transformation exhibited excellent functional group tolerance, accommodating diverse substituents including aryl (**NC-1** to **NC-3**), amine (**NC-4** and **NC-5**), urea (**NC-6**), amide or hydroxyl (**NC-7** to **NC-11**), and ester (**NC-12**) groups (Scheme 3).

Our previous studies demonstrated that amino modification can significantly enhance the anti-tumor activity of β-caryolane derivatives.[24] However, such amino-alkynes are not readily

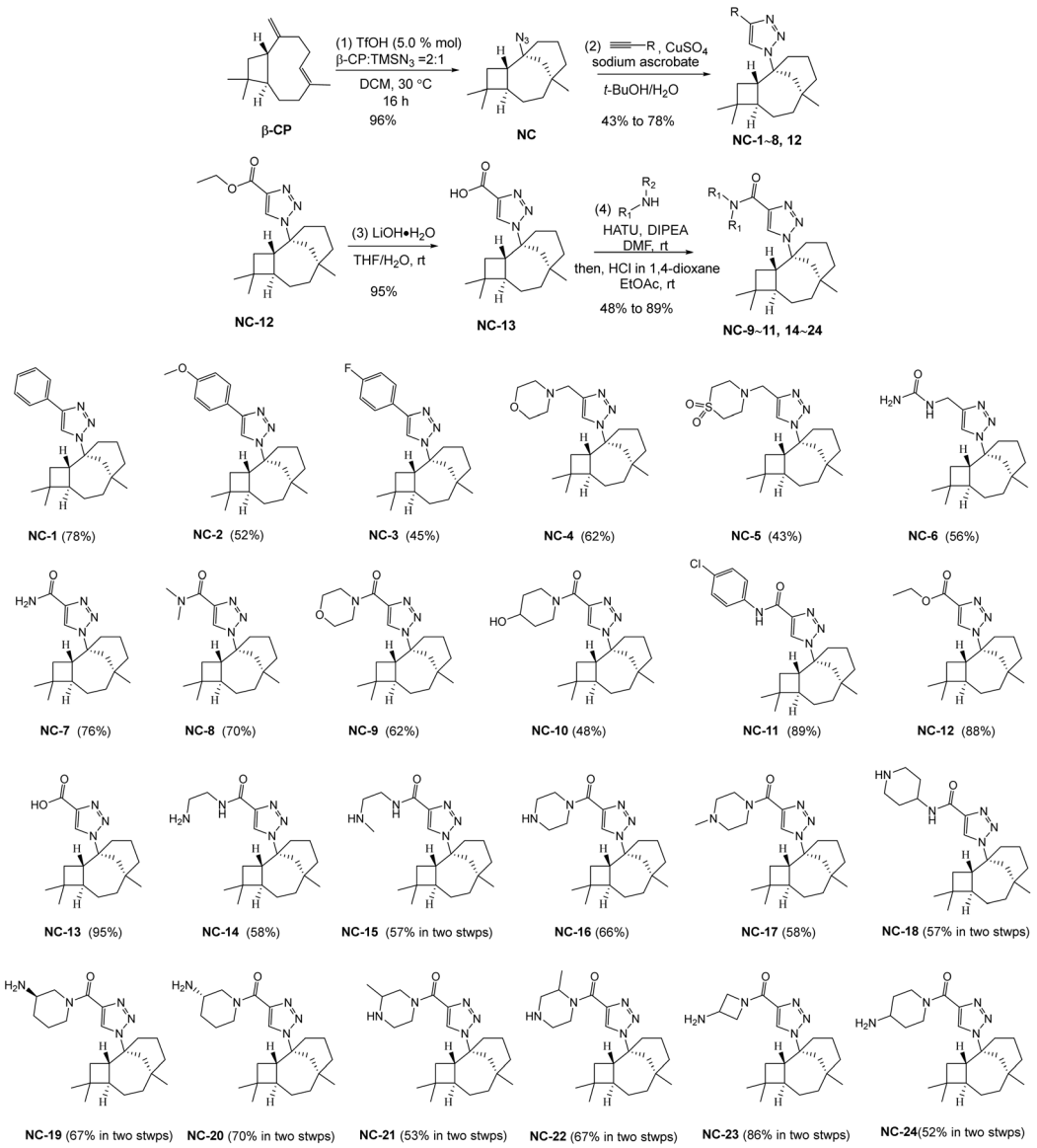

Scheme 3 Hydroazidation reaction of β-CP with $TMSN_3$, click reactions of β-caryolane-azide **NC** with alkynes and amidation reactions of acid **NC-13** with amino substrates. Reaction conditions: (1) $TMSN_3$ (1.0 equiv.), β-CP (2.0 equiv.), TfOH (0.1 equiv.), 30 °C in DCM, 16 h; (2) **NC** (0.2 mmol, 1.0 equiv.), substituted alkynes (0.24 mmol, 1.2 equiv.), $CuSO_4$ (0.004 mmol, 0.02 equiv.), sodium ascorbate (0.002 mmol, 0.1 equiv.), *t*-BuOH/H_2O (5 mL, v/v 4 : 1), room temperature, 12 h; (3) LiOH, THF/H_2O; (4) NHR_1R_2, HATU, DIPEA, DMF; (5) HCl in 1,4-dioxane, EtOAc. The yield was calculated based on the ^1H NMR data with trimethoxybenzene as the internal standard and azide source as the reference.

available commercially or remain synthetically challenging. Therefore, we hydrolyzed **NC-12** to the corresponding acid **NC-13**, which was then employed as a precursor to react with various amine substrates, successfully yielding amino-functionalized products **NC-14** to **NC-24**.

2.2 Pharmacology

2.2.1 β-caryolane derivatives inhibit CRC cell growth. The *in vitro* activity of all β-caryolane derivatives (**SA, CA** and **NC**) was evaluated against three CRC cell lines (HT-29, HCT-116 and HCT-15) and one normal colonic epithelial cell line (NCM-460), 5-fluorouracil (**5-FU**), a first-line chemotherapeutic agent for CRC, was used as a positive control to benchmark the potency and selectivity of these compounds. Initial antiproliferative screening was performed on HT-29 cells at concentrations of 10 and 50 μM. As shown in Table S4, although most **SA** compounds exhibited significant antiproliferative activity at 50 μM, a notable contrast was observed: **SA**s bearing aliphatic amino groups showed considerably higher potency than those with aromatic or alkyl substituents. In contrast, all **CA** compounds exhibited negligible activity at 50 μM. Compared to amides, sulfonamides appeared to exhibit superior antiproliferative effects against HT-29 cells. Within the **NC** series, phenyl-coupled thiazole derivatives (**NC-1-NC-3**) generally exhibited lower activity against HT-29 cell line compared to ester-, amide-, and alkyl-coupled thiazole compounds (**NC-4-NC-13**). The

Table 1 IC_{50} values of selected compounds **SA**, **NC** and **5-FU** determined in three human CRC cell lines and normal human colon cell lines. SI = IC_{50} (NCM-460)/IC_{50} (HT-29). "/", not determined

	IC_{50} (μM)				
Cmpd	HT-29	HCT-116	HCT-15	NCM-460	SI
SA-29	7.30 ± 0.28	30.98 ± 13.81	7.69 ± 0.68	23.69 ± 3.44	3.2
SA-30	11.49 ± 0.48	34.63 ± 17.31	16.88 ± 0.66	28.08 ± 1.30	2.4
SA-31	16.41 ± 0.48	40.58 ± 3.14	16.23 ± 0.56	43.67 ± 5.24	2.7
SA-32	11.75 ± 0.22	28.06 ± 6.55	12.97 ± 1.53	22.67 ± 1.03	1.9
NC-14	45.91 ± 11.06	/	/	/	/
NC-15	8.80 ± 2.00	14.45 ± 1.28	15.56 ± 1.82	33.66 ± 8.14	3.8
NC-16	4.02 ± 0.14	17.94 ± 1.01	11.70 ± 0.85	26.13 ± 3.10	6.5
NC-17	22.04 ± 0.61	22.25 ± 0.87	17.50 ± 1.70	32.98 ± 1.20	1.5
NC-18	3.17 ± 0.24	14.73 ± 1.79	14.93 ± 0.98	18.56 ± 4.58	5.9
NC-19	2.50 ± 0.25	14.49 ± 2.57	12.28 ± 0.30	20.26 ± 6.09	8.1
NC-20	3.37 ± 0.22	9.76 ± 0.83	7.04 ± 0.55	8.06 ± 0.68	2.4
NC-21	4.94 ± 0.58	16.33 ± 1.53	11.22 ± 0.26	17.62 ± 6.14	3.6
NC-22	4.08 ± 0.41	13.23 ± 1.67	12.339 ± 0.45	21.58 ± 5.91	5.3
NC-23	7.11 ± 0.44	13.69 ± 1.41	15.30 ± 1.34	18.72 ± 12.95	2.6
NC-24	6.05 ± 0.75	14.32 ± 1.91	15.31 ± 3.38	15.39 ± 1.51	2.5
5-FU	3.63 ± 0.611	1.38 ± 0.21	13.31 ± 2.01	3.94 ± 1.41	1.1

introduction of basic amino groups into ester-coupled thiazole compounds (**NC-14-NC-24**) resulted in significantly enhanced potency. The median inhibitory concentration (IC_{50}) of these high active compounds after 72 hours of incubation with HT-29 cells were determined and summarized in Table 1.

Data analysis of Table 1 further revealed that both **NC-16** and **NC-17**, in which the endocyclic −O− or exocyclic –OH groups (present in **NC-7** or **NC-8**, respectively) were replaced with –NH– or $–NH_2$ moieties, exhibited substantially enhanced antiproliferative activity. This result further highlights the crucial role of amino substituents for antiproliferative activity. Furthermore, comparative analysis revealed that the most of the rigid cyclic amino compounds (**NC-16-NC-24**) showed superior activity compared to their flexible linear counterparts (**NC-14** and **NC-15**), and the tertiary amine compound **NC-17** showed lower activity relative to its primary and secondary amine analogues (**NC-16** and **NC-18-NC-24**). Among these, compound **NC-19** displayed the highest antiproliferative activity with an IC_{50} of 2.50 ± 0.25 μM against HT-29 cell line.

The active β-cyclohexane derivatives were further evaluated in two additional human CRC cell lines, HCT-116 and HCT-15. The results demonstrated that these compounds also significantly inhibited the proliferation of both HCT-116 and HCT-15 cells, but their inhibitory effects on HT-29 cells remained more potent in comparison (Table 1). A major limitation of many antitumor drugs is their lack of selectivity between cancer and normal cells.[34] Therefore, we evaluated the cytotoxicity of the compounds in Table 1 against the normal human colon cell line NCM-460 to determine their selectivity index (SI), defined as the ratio of cytotoxicity in NCM-460 cells to that in cancer cells. As shown in Table 1, compound **NC-19** demonstrated the highest selectivity (SI = 8.1) toward HT-29 cells over NCM-460 cells. This selectivity was significantly greater than that of **5-FU**. Considering activity and selectivity, compounds **NC-19** were selected for further pharmacological studies on HT-29 cells.

2.2.2 NC-19 induced apoptosis in HT-29 cells. The antiproliferative effect of **NC-19** on HT-29 cells was evaluated using a colony formation assay. As showed in Fig. 2A and B, a significant reduction in the number of colonies formed by HT-29 cells was observed following treatment with **NC-19** for 72 hours. Meanwhile, several typical morphological features of apoptosis, such as cell shrinkage and the formation of apoptotic bodies, were observed in the **NC-19**-treated HT-29 cells (Fig. 2C), suggesting that **NC-19** may induce apoptosis. To further confirm this effect, flow cytometry assay was performed. As shown in Fig. 2D and E, after 48 hours of treatment with **NC-19**, the percentage of apoptotic HT-29 cells gradually increased in a dose-dependent manner (11.25%, 11.92%, 26.69%, and 69.53%, respectively), with a notable rise in both early and late apoptotic populations. Western blot analysis was performed to examine the expression of key apoptosis-related proteins. The results showed a significantly upregulation of cleaved caspase-3 and cleaved PARP1, while the levels of total caspase-3 and PARP1 remained unchanged (Fig. 2F and G), suggesting that **NC-19** effectively activates the apoptotic pathway. Additionally, the effect of pan-caspase inhibitor Z-VAD-FMK on preventing **NC-19** induced cell death was also examined. Pretreating with Z-VAD-FMK for 8 hours, followed by treatment with **NC-19** for 72 hours, increased HT-29 cell viability from 73.64% to 96.00% (Fig. 2H). Taken together, these results demonstrate that **NC-19** induces apoptosis in HT-29 cells.

2.2.3 NC-19 induced cell cycle arrest and ROS generation in HT-29 cells. To further investigate the antiproliferative mechanism of **NC-19**, cell cycle arrest assays were performed using flow cytometry and western blot. As shown in Fig. 3A and B, the percentage of cells in the G0/G1 phase increased from 52.00% to 65.27% in a dose-dependent manner after 24 hours of treatment with **NC-19**. The transition from G1 to S phase requires the participation of multiple kinases and phosphatases, among which the activated CDK2/Cyclin E complex plays a crucial

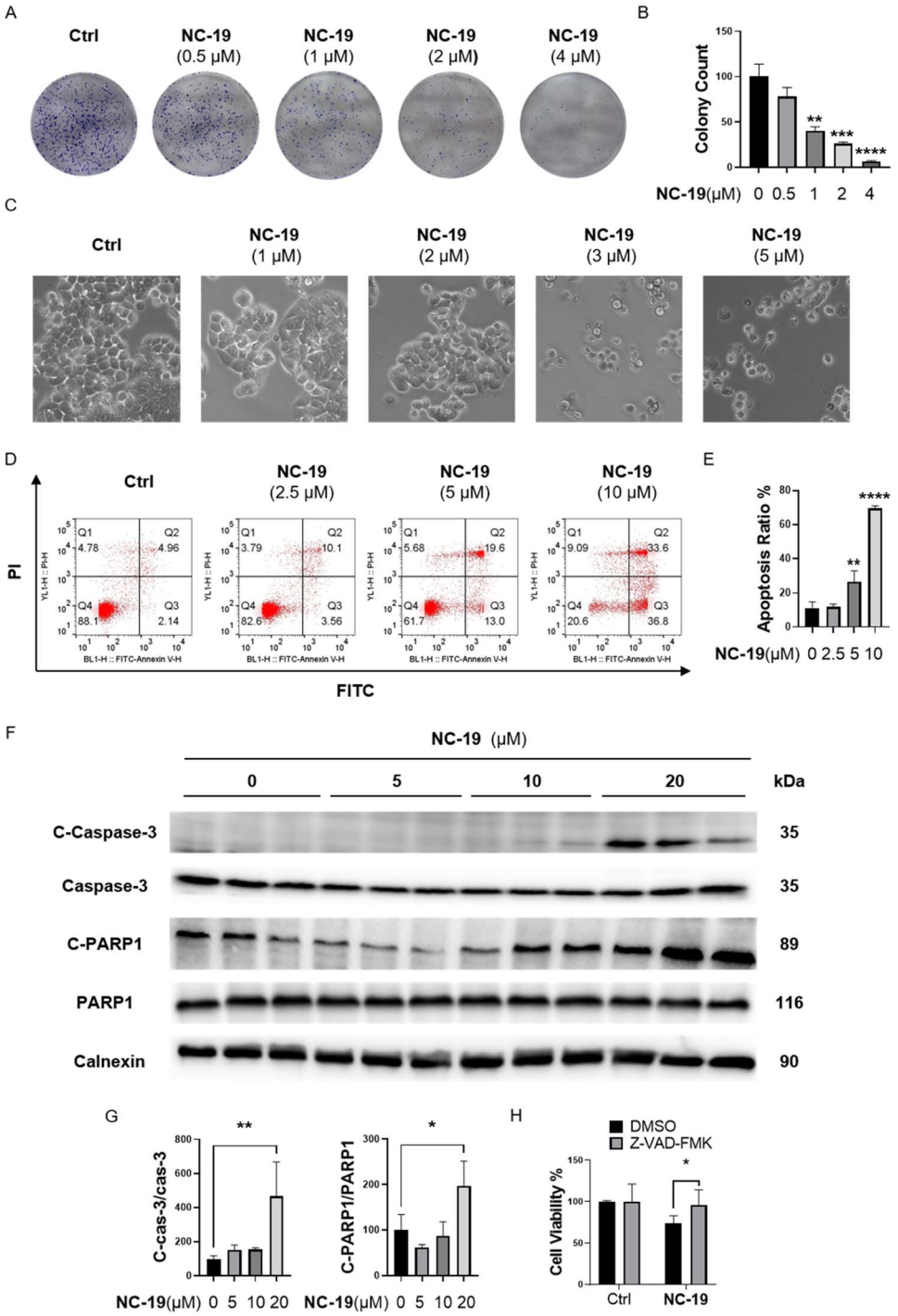

Fig. 2 NC-19 induced apoptosis of HT-29 cells. (A and B) The clonogenic potential of HT-29 cells was observed following treatment with NC-19 (0, 0.5, 1, 2, 4 μM) for 72 hours by specific protocols *in vitro*. Colonies (consisting of over 50 cells) were quantified. (C) Morphology changes of HT-29 cells after treatment with NC-19 (1–5 μM) for 72 hours. (D and E) Flow cytometry analysis of apoptosis in HT-29 cells after treatment with NC-19 (0, 2.5, 5, 10 μM) for 24 hours. (F and G) Western blot and bar graph analysis of cleaved caspase-3, caspase-3, cleaved PARP1 and PARP1 protein expression after treatment with NC-19 (0, 5, 10, 20 μM) for 24 hours in HT-29 cells. (H) Cell viability of HT-29 cells pretreatment with Z-VAD-FMK for 8 hours, followed by exposure to NC-19 for 72 hours.

initiating role. As demonstrated in Fig. 3C and D, NC-19 treatment significantly reduced the expression levels of both CDK2 and Cyclin E. These results suggested that NC-19 induces G0/G1 phase cell cycle arrest by downregulating key cell cycle regulatory proteins.

Intracellular ROS levels must be maintained within an appropriate range to support normal cellular physiological function and survival, excessive ROS can induce oxidative damage and lead to various forms of cell death, including apoptosis. To investigate the involvement of ROS in NC-19-

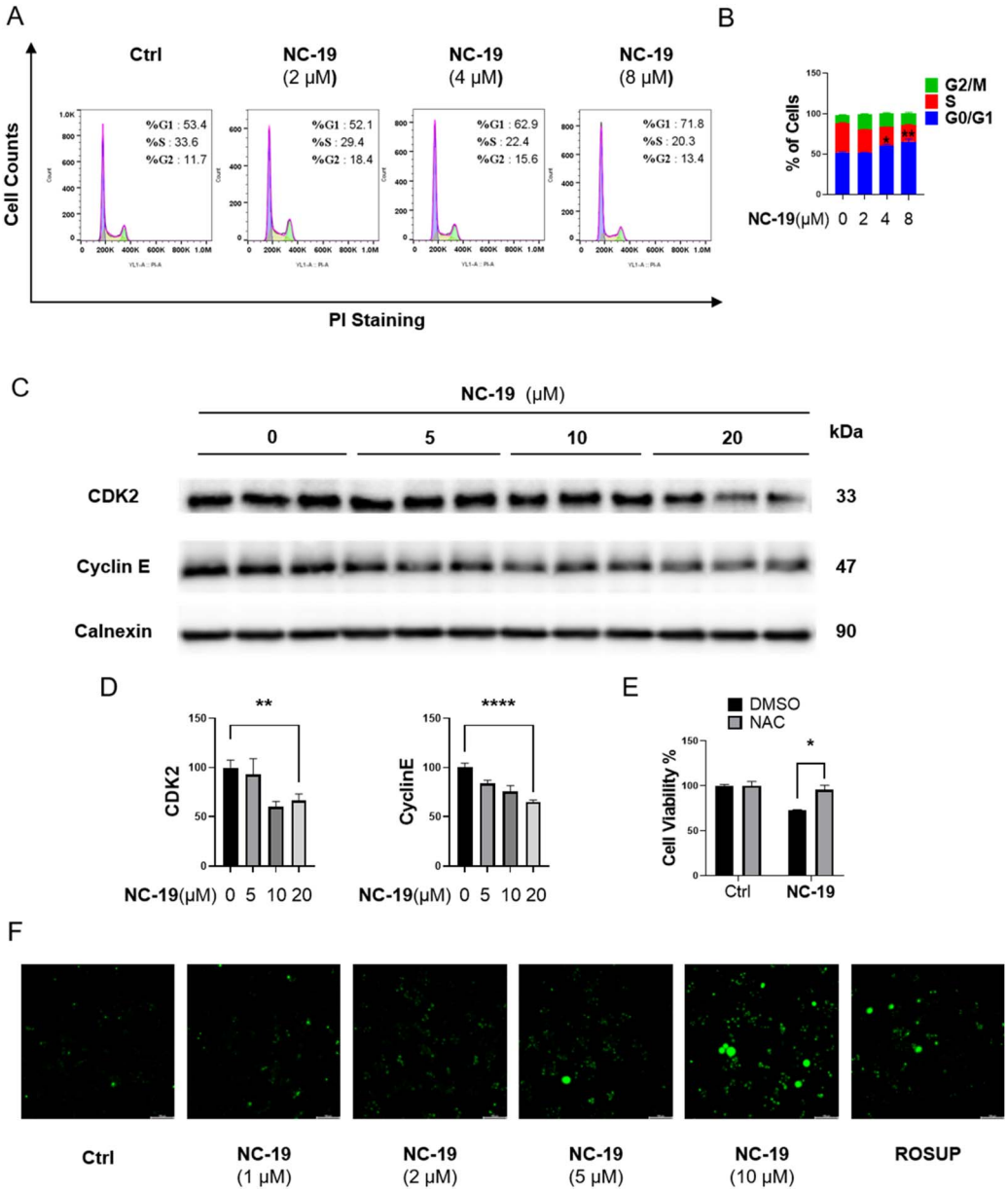

Fig. 3 **NC-19** induces HT-29 G0/G1 phase cell cycle arrest and ROS generation. (A and B) Cell cycle analysis of HT-29 cell cycle distribution after treatment with **NC-19** (0, 2, 4, 8 μM) for 24 hours. (C and D) Western blot and bar graph analysis of CDK2 and Cyclin E protein expression in HT-29 cells after treatment with **NC-19** (0, 5, 10, 20 μM) for 24 hours. (E) Cell viability of HT-29 cells pretreated with **NAC** (2 mM) for 8 hours, followed by incubation with or without 2 μM **NC-19** for 72 hours. (F) Detection of ROS generation by DCFH-DA in HT-29 cells after treatment with **NC-19** (0, 1, 2, 5, 10 μM) for 24 hours.

induced cell death, HT-29 cell was pretreated with the ROS scavenger NAC for 8 hours prior to a 72 hour exposure to **NC-19**. This pretreatment increased cell viability from 72.56% to 95.41% (Fig. 3E). Furthermore, to determine whether **NC-19** disrupts redox homeostasis in the HT-29 cells, we evaluated intracellular ROS production using confocal microscopy with DCFH-DA as a fluorescent probe. As demonstrated in Fig. 3F, **NC-19** treatment markedly increased ROS generation. Collectively, these findings suggest that **NC-19** triggers both G0/G1 cell cycle arrest and ROS accumulation in HT-29 cells.

2.2.4 NC-19 suppresses HT-29 cells migration. Tumor metastasis is a hallmark of malignancy and a major cause of cancer recurrence and mortality.[35] Consequently, inhibiting metastatic progression represents a crucial therapeutic objective. To evaluate the effect of **NC-19** on HT-29 cell migration, a wound healing assay was performed. As shown in Fig. 4A and B, after 24 h of treatment, the recovery area of the wound significantly decreased in a concentration-dependent manner after treatment with **NC-19** for 24 h. Since cell migration capability is closely linked to extracellular matrix (ECM) remodeling, we investigated MMP9, a key protein that promotes tumor

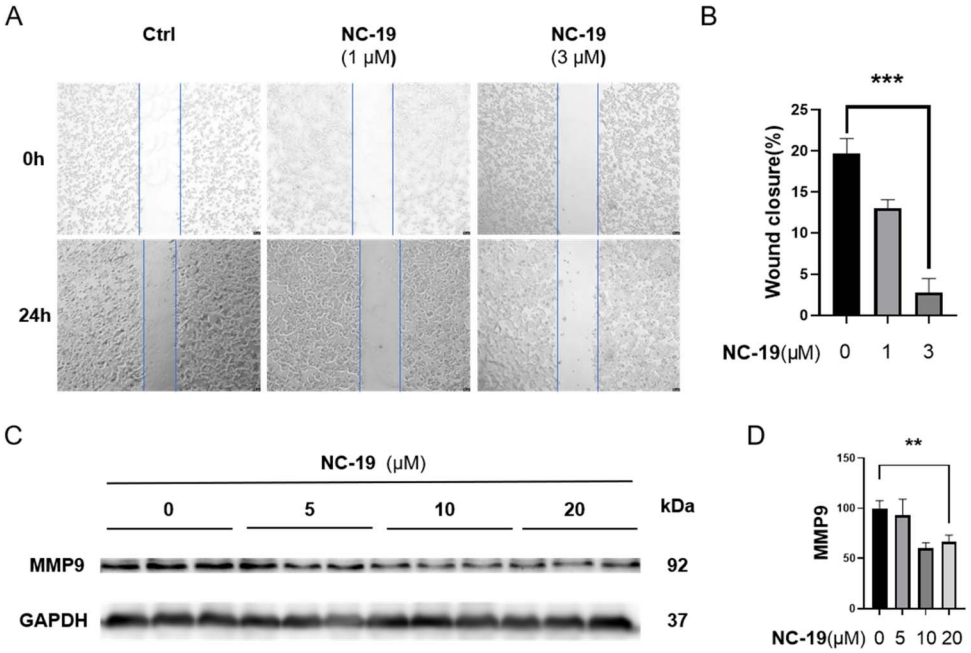

Fig. 4 Effect of **NC-19** on HT-29 cell migration. (A and B) Images and bar graph analysis of the wound closure of HT-29 cells after treatment with **NC-19** (0, 1, 3 μM) for 24 hours. (C and D) Western blot and bar graph analysis of MMP9 protein expression in HT-29 cells after treatment with **NC-19** (0, 5, 10, 20 μM) for 24 hours.

progression by degrading the ECM and is critical for cancer invasion and metastasis.[36,37] Western blot analysis revealed that MMP9 expression decreased in a concentration-dependent manner after treatment with **NC-19** (Fig. 4C and D). Together, these findings demonstrate that **NC-19** effectively suppresses HT-29 cell migration.

3 Conclusion

In summary, this study successfully extends the acid-catalyzed addition-rearrangement reaction of β-CP to direct reactions with sulfonamides, amides, and azides. This strategy features mild conditions and excellent functional group compatibility, significantly enriching the structural diversity of β-CP derivatives. Notably, the β-CP-azide synthesized *via* this method serves as a versatile module for Click chemistry, enabling rapid construction of more complex β-CP derivatives and laying a solid material foundation for the functionalization and application of this class of molecules. In the biological evaluation, we systematically investigated the *in vitro* antiproliferative activity of β-CP derivatives against CRC cell lines. Structure–activity relationship analysis revealed that the introduction of an amino group significantly enhances antiproliferative efficacy. Furthermore, these compounds exhibited superior antiproliferative activity against HT-29 cell line compared to HCT-116 and HCT-15 cell lines. Among them, the most active compound **NC-19**, could induce G0/G1 phase arrest and elevate intracellular ROS levels, thus trigger apoptosis of HT-29 cells. This study not only advances the synthetic methodology of β-CP-based compounds but also provides a promising lead compound for the development of novel anti-CRC therapeutics, demonstrating considerable application potential.

4 Experimental section

4.1 Chemistry

NMR spectra (^{1}H and ^{13}C) were recorded on a Bruker AVANCE spectrometer operating at 400 or 600 MHz. Chemical shifts (δ) are reported in parts per million (ppm) using tetramethylsilane (TMS) as an internal standard. Mass spectrometry data were acquired using a QDA mass detector was used; for high-resolution mass spectrometry (HRMS), an Agilent 1290 Infinity LC coupled to an Agilent 6540 Q-TOF mass spectrometer with an electrospray ionization (ESI) source was employed. Compound purification was performed by flash chromatography using silica gel (200–300 mesh, Qingdao Haiyang Chemical Co., Ltd). All commercially available reagents and solvents (from Sinopharm Chemical Reagent Co., Ltd) were used as received, unless otherwise noted. Anhydrous solvents were prepared according to standard laboratory methods. The reported yields refer to isolated products and were not optimized.

4.2 Chemical synthesis

4.2.1 TfOH catalysed addition reaction of β-caryophyllene

4.2.1.1 Condition optimization of acid-catalyzed addition reaction of β-caryophyllene. A flask equipped with a septum and a magnetic stir bar was charged with substituted *p*-toluenesulfonamide (0.1 mmol), β-CP (X mmol) and solvent (2.0 mL) under nitrogen atmosphere. Then acid was slowly added to the

mixture. The mixture was stirred at 30 °C for 16 hours and concentrated. 1,3,5-Trimethoxybenzene (0.033 mmol) was added, and the ^{1}H-NMR was detected. The yield of hydroamination was determined by internal standard method.

4.2.1.2 General procedure A for the synthesis of SA. A flask equipped with a septum and a magnetic stir bar was charged with substituted sulfonamide (0.1 mmol), β-CP (0.2 mmol) and 1,4-dioxane (2.0 mL) under air atmosphere. Then TfOH (0.44 μL, 5.0 mol%) was slowly added to the mixture. The mixture was stirred at 30 °C for 16 hours and concentrated. The residue was purified by column chromatography (silica gel, hexane/EtOAc) to give the product.

4.2.1.3 General procedure B for the synthesis of CA. A flask equipped with a septum and a magnetic stir bar was charged with substituted amide (0.1 mmol), β-CP (0.5 mmol) and dichloromethane (2.0 mL) under air atmosphere. Then TfOH (0.88 μL, 10.0 mol%) was slowly added to the mixture. The mixture was stirred at 30 °C for 16 hours and concentrated. The residue was purified by column chromatography (silica gel, hexane/EtOAc) to give the product.

4.2.1.4 The synthesis of NC. A flask equipped with a septum and a magnetic stir bar was charged with azidotrimethylsilane (5.0 mmol), β-CP (10.0 mmol), and dichloromethane (25.0 mL) under air atmosphere. Then TfOH (22.0 μL, 5.0 mol%) was slowly added to the mixture. The mixture was stirred at 30 °C for 16 hours, then the reaction mixture was successively washed with saturated aq. $NaHCO_3$ and saturated brine and concentrated. The residue was purified by column chromatography (silica gel, hexane/EtOAc) to give **NC** as colorless oil with 96% isolation yield.

4.2.1.5 General procedure C for the synthesis of NC1-8 and 12. A flask equipped with a septum and a magnetic stir bar was charged with **NC** (0.2 mmol), substituted alkynes (0.24 mmol) and *t*-BuOH/H_2O (5 mL, v/v 4 : 1), then $CuSO_4$ (0.004 mmol) and Sodium ascorbate (0.002 mmol) were sequentially added, followed by stirring at 25 °C for 16 hours. EtOAc was added, then washed with water and brine, dried and concentrated. The residue was purified by column chromatography (silica gel, hexane/EtOAc) to give the product.

4.2.1.6 General procedure D for the synthesis of NC9-11 and 14–24. A flask equipped with a septum and a magnetic stir bar was charged with **NC** (0.1 mmol), amine (0.15 mmol), DIPEA (0.3 mmol) and dichloromethane (3.0 mL) under nitrogen atmosphere. Then HATU (0.12 mmol) was added to the mixture. The mixture was stirred at 25 °C for 12 hours, and 20 mL DCM was added, and then washed with water and brine, dried and concentrated. Then EtOAc (5 mL) was added and a HCl 1,4-dioxane solution (2 mL, 4 mmol) was added, and stirred at 25 °C for 2 hours. Concentrated and the mixture was neutralized with saturated aqueous $NaHCO_3$, extracted with EtOAc, dried (anhyd. Na_2SO_4), and concentrated under reduced pressure. The residue was purified by column chromatography (silica gel, DCM/MeOH) to give the product.

4.2.1.7 X-ray structure determination. A suitable crystal of **SA-1** (0.33 × 0.38 × 0.36 mm^3) was selected and mounted on a Bruker D8 venture microsource diffractometer. Data were measured using monochromatic Mo-Ka radiation at $T = 100$ K. Data reduction, scaling and absorption corrections were performed using SAINT (Bruker, V8.38A, 2013). The structure was solved with the shelXT (Sheldrick, 2015) structure solution program using the Intrinsic Phasing solution method and by using Olex2 (Dolomanov *et al.*, 2009) as the graphical interface. The model was refined with version 2018/3 of ShelXL (Sheldrick, 2008) using LeastSquares minimisation.

4.3 Biology

4.3.1 Reagents and cell lines. HT-29 (SCSP-5032), HCT-116 (SCSP-5076), and HCT15 (TCHu133) were obtained from National Collection of Authenticated Cell Cultures (Shanghai, China). Normal cell line NCM-460 (iCell-h373) was obtained from Cellverse Co., Ltd (Shanghai, China). CCK-8 and Z-VAD-FMK was purchased from Meilunbio (Dalian, China). 5-FU was purchased from Yuanye Biotechnology (Shanghai, China). NAC, DCFH-DA, RIPA lysis buffer, protease inhibitors, phosphatase inhibitors, 4% paraformaldehyde fix solution, hematoxylin and eosin staining kit, Western blocking buffer, Enhanced BCA protein assay kit, SDS-PAGE gel kit, BeyoECL Plus kit, Annexin V-FITC cell apoptosis detection kit and PI cell cycle detection kit were purchased from Beyotime Biotechnology (Shanghai, China). TBST buffer, glycine, Tris and SDS were purchased from Solarbio (Beijing, China). The primary antibodies were as follows: caspase-3 (CST, 14220T), cleaved caspase-3 (CST, 9664T), PARP1 (CST, 9532T), cleaved PARP1 (CST, 5625T), GAPDH (CST, 2118T), CDK2 (Proteintech, 10122-1-Ap), cyclin E (Proteintech, 11554-1-Ap), MMP9 (Proteintech, 10375-2-Ap), calnexin (Proteintech, 10427-1-Ap), tubulin (Proteintech, 10094-1-Ap). The secondary antibodies were as follows: HRP-labeled goat anti-Rabbit (Proteintech, SA00001-2) and anti-Mouse IgG (Proteintech, SA00001-1).

4.3.2 Cell culture and anti-proliferation assay. NCM-460 cells were cultured in RPMI 1640 medium, HT-29, HCT-116 and HCT-15 cells were cultured in McCoy's 5A medium. All media were supplemented with 10% FBS and 1% penicillin-streptomycin, and cells were maintained in 5% CO_2 incubator at 37 °C. HT-29 cells were digested and plated into 24 well plates (8000 cells per well) and incubated overnight. HT-29, HCT-116, HCT-15 and NCM-460 Cells were plated into 96-well plates (4 × 10^3 cells per well) and incubated overnight. Different concentrations of 5-FU and β-Caryolane derivatives were added after cell adherence. After 72 h treatment, old media were replaced with fresh media containing 10% CCK-8. After 1 h incubation at 37 °C, absorbance at 450 nm was measured. Cell survival rate (%) = OD of the dosing group/OD of the control group × 100%. IC_{50}: the concentration of compounds that can cause 50% inhibition of cell viability.

4.3.3 Morphological observation of HT-29 cells. HT-29 cells (8 × 10^3 cells per well) were digested and plated into 24 well plates and incubated overnight. Different concentrations of **NC-19** (1, 2, 3, or 5 μM) or DMSO (control) were added to each well, and after 72 h, cell morphology was observed using an inverted microscope (Leica, German).

4.3.4 Z-VAD-FMK and NAC inhibition assay. HT-29 cells (4 × 10^3 cells per well) were seeded into 96 well plates and

pretreated with 100 μM Z-VAD-FMK or 2 mM NAC for 8 hours. Cells were then treated with 0.5 μM **NC-19** or DMSO (control) for 72 h, and cell viability was measured using the CCK-8 assay. Absorbance at 450 nm was recorded after 1 h incubation at 37 °C.

4.3.5 Colony formation assay. HT-29 Cells (1×10^3 cells per well) were seeded into 6-well plates and incubated overnight. The cells were then exposed to **NC-19** (0.5, 1, 2, 4 μM) or DMSO (control) for an additional 72 h. Subsequently, the media were replaced with fresh complete culture media (twice a week). After 10 days, the colonies were fixed with 4% paraformaldehyde for 15 min at 25 °C and stained with a 0.5% crystal violet solution for 30 min at 25 °C. Colonies containing 50 or more cells were counted.

4.3.6 Wound healing assay. HT-29 cells (1×10^6 cells per well) were seeded into 6-well plates and incubated overnight. A scratch wound was created in the cell monolayer using a 200 μL pipette tip. The medium was then removed, and washed with PBS. Cells were exposed to with **NC-19** (1, 3 μM) or DMSO (control). Images of the cells were taken at 0 and 24 h with an inverted microscope (Leica, German) at 10× magnification and analyzed with ImageJ (National Institute of Health, Maryland, USA). The migration rate was calculated using the following formula: wound closure % $= (S_{0h} - S_{24h})/S_{0h} \times 100\%$.

4.3.7 Cell apoptosis assay. HT-29 cells (2×10^5 cells per well) were seeded in 6-well plates and incubated overnight. The cells were then exposed to **NC-19** (2.5, 5, 10 μM) or DMSO (control) for 72 h. Cells were stained with Annexin V-FITC and PI for 20 min, after staining, the cells were detected and analyzed using a flow cytometry.

4.3.8 Cell cycle assay. HT-29 cells (1.2×10^5 cells per well) were plated into 6-well plates and incubated overnight. The cells were then treated with **NC-19** (2, 4, 8 μM) or DMSO (control) for 24 hours, and fixed in 70% ethanol at 4 °C for 2 hours. Cells were then stained with PI and Rnase for 0.5 hours. After staining, the cells were detected and analyzed using a flow cytometry.

4.3.9 Determination of intracellular ROS. HT-29 cells (1×10^4 cells per well) were seeded in 96 well plates and incubated overnight. The cells were then treated with **NC-19** (1, 2, 5, 10 μM) or DMSO (control) for 24 hours, stained with DCFH-DA to detect ROS, with green fluorescence observed using an inverted fluorescence microscope (Leica, Germany).

4.3.10 Western Blot assay. HT-29 cells (1×10^6 cells per well) were seeded into 6 well plates and incubated overnight. Cells were treated with **NC-19** (5, 10, 20 μM) or DMSO (control) for 24 hours, lysed using RIPA lysis buffer with protease and phosphatase inhibitors, and the supernatants were collected after centrifugation (15000g × 10 min at 4 °C). Total protein was measured using the Enhanced BCA protein assay kit. Equal amounts of protein (25 μg) were loaded onto SDS-PAGE gels, transferred to PVDF membranes, and blocked for 1 hour. Membranes were incubated with primary antibodies overnight at 4 °C, washed three times, and then incubated with secondary antibodies for 1 hour, followed by three additional washes. Protein bands were visualized using the BeyoECL Plus kit on a ChemiDoc XRS+ system (Bio-Rad, USA) and quantified using the ImageJ (NIH, USA).

4.3.11 Statistical analysis. Statistical analysis was analyzed by one-way analysis of variance followed by the Dunnett test using GraphPad Prism software. Data were shown as average ± standard deviation. Independent experiments were performed at least three times. *$p < 0.05$; **$p < 0.01$; ***$p < 0.001$, ****$p < 0.0001$ compared with control (compare all columns *vs.* control column).

Conflicts of interest

There are no conflicts to declare.

Data availability

All relevant data are within the manuscript and its additional files.

CCDC 1942093 contains the supplementary crystallographic data for this paper.[38]

Supplementary information (SI): includes the optimization of acid-catalyzed reaction conditions, as well as NMR and HRMS spectra of the synthesized compounds. See DOI: https://doi.org/10.1039/d5ra07312j.

Acknowledgements

This work was supported by the Jiangxi Provincial Natural Science Foundation (20252BAC240504).

References

1 F. Bray, M. Laversanne, H. Sung, J. Ferlay, R. L. Siegel, I. Soerjomataram and A. Jemal, *Ca-Cancer J. Clin.*, 2024, **74**, 229–263.
2 N. Li, B. Lu, C. Luo, J. Cai, M. Lu, Y. Zhang, H. Chen and M. Dai, *Cancer Lett.*, 2021, **522**, 255–268.
3 J. Guinney, R. Dienstmann, X. Wang, A. de Reynies, A. Schlicker, C. Soneson, L. Marisa, P. Roepman, G. Nyamundanda, P. Angelino, B. M. Bot, J. S. Morris, I. M. Simon, S. Gerster, E. Fessler, E. M. F. De Sousa, E. Missiaglia, H. Ramay, D. Barras, K. Homicsko, D. Maru, G. C. Manyam, B. Broom, V. Boige, B. Perez-Villamil, T. Laderas, R. Salazar, J. W. Gray, D. Hanahan, J. Tabernero, R. Bernards, S. H. Friend, P. Laurent-Puig, J. P. Medema, A. Sadanandam, L. Wessels, M. Delorenzi, S. Kopetz, L. Vermeulen and S. Tejpar, *Nat. Med.*, 2015, **21**, 1350–1356.
4 E. Dekker, P. J. Tanis, J. L. A. Vleugels, P. M. Kasi and M. B. Wallace, *Lancet*, 2019, **394**, 1467–1480.
5 J. Haynes and P. Manogaran, *Int. J. Mol. Sci.*, 2025, **26**, 1988.
6 J. Khazir, D. L. Riley, L. A. Pilcher, P. De-Maayer and B. A. Mir, *Nat. Prod. Commun.*, 2014, **9**, 1655–1669.
7 D. J. Newman and G. M. Cragg, *J. Nat. Prod.*, 2020, **83**, 770–803.
8 Z. Wang, X. Xu, H. Wen, Z. Qiao, H. Zhou, L. Chen, Y. Ge, Y. Wang, Y. Han, Y. Zhao and X. Liang, *Bioorg. Chem.*, 2025, **166**, 109103.

9 M. Sköld, A. T. Karlberg, M. Matura and A. Börje, *Food Chem. Toxicol.*, 2006, **44**, 538–545.
10 J. Gertsch, M. Leonti, S. Raduner, I. Racz, J. Z. Chen, X. Q. Xie, K. H. Altmann, M. Karsak and A. Zimmer, *P. Natl. Acad. Sci. USA*, 2008, **105**, 9099–9104.
11 K. R. Park, D. Nam, H. M. Yun, S. G. Lee, H. J. Jang, G. Sethi, S. K. Cho and K. S. Ahn, *Cancer Lett.*, 2011, **312**, 178–188.
12 K. Fidyt, A. Fiedorowicz, L. Strzadala and A. Szumny, *Cancer Med.*, 2016, **5**, 3007–3017.
13 S. S. Dahham, Y. M. Tabana, M. A. Iqbal, M. B. K. Ahamed, M. O. Ezzat, A. S. A. Majid and A. M. S. A. Majid, *Molecules*, 2015, **20**, 11808–11829.
14 C. Kim, S. K. Cho, K. D. Kim, D. Nam, W. S. Chung, H. J. Jang, S. G. Lee, B. S. Shim, G. Sethi and K. S. Ahn, *Apoptosis*, 2014, **19**, 708–718.
15 S. S. Dahham, Y. Tabana, M. Asif, M. Ahmed, D. Babu, L. E. Hassan, M. B. K. Ahamed, D. Sandai, K. Barakat, A. Siraki and A. Majid, *Int. J. Mol. Sci.*, 2021, **22**, 10550.
16 Y. V. Gyrdymova and S. A. Rubtsova, *Chem. Pap.*, 2022, **76**, 1–39.
17 J. Legault and A. Pichette, *J. Pharm. Pharmacol.*, 2007, **59**, 1643–1647.
18 G. C. Segat, M. N. Manjavachi, D. O. Matias, G. F. Passos, C. S. Freitas, R. Costa and J. B. Calixto, *Neuropharmacology*, 2017, **125**, 207–219.
19 E. P. Romanenko and A. V. Tkachev, *Russ. Chem. Bull.*, 2018, **67**, 1051–1058.
20 E. J. Corey, R. B. Mitra and H. Uda, *J. Am. Chem. Soc.*, 1964, **86**, 485.
21 E. J. Corey, H. Uda and R. B. Mitra, *J. Am. Chem. Soc.*, 1963, **85**, 362.
22 O. I. Yarovaya, D. V. Korchagina, T. V. Rybalova, Y. V. Gatilov, M. P. Polovinka and A. Barkhash, *Russ. J. Org. Chem.*, 2004, **40**, 1593–1598.
23 F. Tang, R. Bian, Q. Xie and H. Zhou, *Zhongguo Yaolixue Tongbao*, 1991, **7**, 147–148.
24 Z. W. Wang, Y. Chen, A. J. Huang, H. Wen, Y. T. Wu, X. J. Xu, Z. J. Qiao, L. Y. Chen, Y. P. Zhao and X. M. Liang, *RSC Med. Chem.*, 2025, **16**, 3174–3189.
25 L. Fitjer, A. Malich, C. Paschke, S. Kluge, R. Gerke, B. Rissom, J. Weiser and M. Noltemeyer, *J. Am. Chem. Soc.*, 1995, **117**, 9180–9189.
26 M. M. B. Silva, C. G. Vieira and K. A. da Silva Rocha, *Mol. Catal.*, 2023, **547**, 113302.
27 K. P. Volcho, L. E. Tatarova, E. V. Suslov, D. V. Korchagina, N. F. Salakhutdinov and V. A. Barkhash, *Russ. J. Org. Chem.*, 2001, **37**, 1418–1429.
28 K. A. D. Rocha, N. V. S. Rodrigues, I. V. Kozhevnikov and E. V. Gusevskaya, *Appl. Catal. A-Gen.*, 2010, **374**, 87–94.
29 V. V. Fomenko, D. V. Korchagina, N. F. Salakhutdinov and V. A. Barkhash, *Helv. Chim. Acta*, 2001, **84**, 3477–3487.
30 O. I. Yarovaya, K. S. Kovaleva, S. S. Borisevich, T. V. Rybalova, Y. V. Gatilov, E. O. Sinegubova, A. S. Volobueva, V. V. Zarubaev and N. F. Salakhutdinov, *Mendeleev Commu.*, 2022, **32**, 609–611.
31 J. Fei, Z. Wang, Z. R. Cai, H. Sun and X. Cheng, *Adv. Synth. Catal.*, 2015, **357**, 4063–4068.
32 K. A. D. Rocha, N. V. S. Rodrigues, I. V. Kozhevnikov and E. V. Gusevskaya, *Appl Catal a-Gen*, 2010, **374**, 87–94.
33 P. Thirumurugan, D. Matosiuk and K. Jozwiak, *Chem. Rev.*, 2013, **113**, 4905–4979.
34 G. K. Dy and A. A. Adjei, *Ca-Cancer J. Clin.*, 2013, **63**, 249–279.
35 I. J. Fidler, *Nat. Rev. Cancer*, 2003, **3**, 453–458.
36 G. Bergers, R. Brekken, G. McMahon, T. H. Vu, T. Itoh, K. Tamaki, K. Tanzawa, P. Thorpe, S. Itohara, Z. Werb and D. Hanahan, *Nat. Cell Biol.*, 2000, **2**, 737–744.
37 W. Liu, Y. Yu, T. Hou, H. Wei, F. Lv, A. Shen, Y. Liu, J. Wang and D. Fu, *Chem. Biol. Interact.*, 2024, **398**, 111113.
38 CCDC 1942093, Experimental Crystal Structure Determination, 2025, DOI: 10.5517/ccdc.csd.cc235x5d.